Supplementary Table 1. Properties of currently available monomeric NIR FPs engineered from bacterial phytochromes with demonstrated mammalian live-cell applications and parental dimeric iRFP720.

NIR FP	Initial bacterial phytochrome	Ex, nm	Em, nm	Extinction coefficient, M^{-1} cm^{-1}	Quantum yield, %	Molecular brightness *vs.* iRFP713, %	Photostability in mammalian cells, $t_{1/2}$, s	p*K*a	Brightness in HeLa cells *vs.* iRFP713, % [a]	Reference
miRFP670	RpBphP1	642	670	87,400	14.0	198	490	4.5	72	[10]
miRFP703		674	703	90,900	8.6	127	650	4.5	37	
miRFP709		683	709	78,400	5.4	69	500	4.5	30	
mIFP [b]	BrBphP	683 (683)	705 (704)	65,900 (82,000)	6.9 (8.4)	74	90	4.5	15	[50]
miRFP720	RpBphP2	702	720	98,000	6.1	97	510	4.5	116	this paper
dimeric iRFP720	RpBphP2	702	720	96,000	6.0	93	490	4.5	112	[9]

[a] Determined as effective NIR fluorescence in transiently transfected live HeLa cells with no supply of exogenous biliverdin and after normalization to fluorescence of co-transfected EGFP. [b] Characteristics of mIFP from the original paper [50] are shown in parentheses.

Supplementary Table 2. P-values for LOV-TRAP-TrioGEF experiments during photoactivation and dark relaxation, from **Figure 5c**.

LOV-TRAP-TrioGEF

Time (s)	P-Values	Time (s)	P-Values
300	0.031891299	600	1.1691E-163
310	9.96935E-86	610	4.6723E-152
320	2.4311E-125	620	1.7478E-145
330	6.4065E-153	630	6.0405E-124
340	2.565E-156	640	1.3387E-102
350	3.5858E-158	650	7.93664E-89
360	1.7684E-167	660	1.3399E-78
370	3.9496E-166	670	3.5994E-65
380	1.3514E-166	680	1.67537E-55
390	1.3597E-162	690	6.61253E-47
400	6.5144E-171	700	7.95978E-45
410	2.1376E-162	710	1.43218E-38
420	1.4995E-167	720	9.48518E-30
430	7.7325E-165	730	1.7476E-27
440	8.8432E-164	740	2.24382E-27
450	6.0304E-174	750	3.93728E-23
460	1.7048E-166	760	3.81733E-19
470	9.107E-171	770	2.49382E-15
480	9.1201E-167	780	1.12901E-17
490	1.121E-164	790	2.4167E-14
500	1.7403E-172	800	1.33476E-11
510	6.7186E-166	810	2.40808E-11
520	8.4263E-163	820	2.55202E-14
530	4.2143E-160	830	4.25168E-07
540	7.7183E-171	840	4.39352E-07
550	4.6737E-166	850	1.30029E-06
560	4.9204E-170	860	3.27316E-08
570	5.8816E-166	870	0.000634557
580	4.5556E-161	880	0.000160235
590	1.3625E-159	890	0.001224826
		900	0.00440346

Supplementary Table 3. P-values from AKAR and JNKAR experiments following stimulation, from **Figures 6c & 6e**.

AKAR		JNKAR	
Time (min)	**P-values**	**Time (min)**	**P-values**
10	2.6166774E-02	10	5.1212650E-01
12	2.8805141E-03	12	1.2391732E-01
14	2.1622749E-06	14	1.7954625E-03
16	3.1379540E-17	16	2.4478761E-13
18	8.6692527E-27	18	4.6282442E-15
20	7.1777612E-36	20	7.1043379E-21
22	4.1836815E-41	22	8.0713200E-30
24	1.1591711E-50	24	3.0477395E-29
26	2.4434264E-46	26	1.7895556E-30
28	5.2413203E-45	28	1.3843044E-30
30	3.1102037E-48	30	9.4405523E-33
32	1.8119585E-51	32	4.5370287E-31
34	1.7959913E-49	34	8.6783552E-30
36	3.6186288E-48	36	9.9012974E-32
38	5.7241214E-50	38	1.0997831E-28
40	5.2799902E-52	40	5.8986294E-29
42	4.3925975E-49	42	9.0189684E-31
44	1.5414714E-50	44	2.0910315E-29
46	6.2866282E-51	46	7.9442567E-31
48	4.6961481E-52	48	3.8508005E-30
50	8.3638525E-56	50	1.2101690E-30
52	1.2624493E-52	52	5.0825045E-29
54	3.7748188E-56	54	7.4706333E-30
56	7.2851581E-56	56	1.7275651E-30
58	6.7707798E-58	58	1.2752226E-31
60	2.5213802E-59	60	2.7664658E-29
62	9.3296663E-59	62	2.9084273E-29
64	1.0037670E-60	64	2.9881099E-30
66	9.0220600E-60	66	4.2749582E-31
68	1.4271111E-56	68	1.5983242E-28
70	3.2723203E-58	70	1.0585313E-29

Supplementary Figure 1. Alignment of the amino acid sequences of miRFP720 with parental dimeric iRFP720 and initial *Rhodopseudomonas palustris* RpBphP2 bacterial phytochrome.

```
           1                                                  50
 RpBphP2   MTEGSVARQPDLSTCDDEPIHIPGAIQPHGLLLALAADMTIVAGSDNLPE
 iRFP720   MAEGSVARQPDLLTCDDEPIHIPGAIQPHGLLLALAADMTIVAGSDNLPE
miRFP720   MAEGSVARQPDLLTCDDEPIHIPGAIQPHGLLLALAADMTIVAGSDNLPE

           51                                                 100
 RpBphP2   LTGLAIGALIGRSAADVFDSETHNRLTIALAEPGAAVGAPIAVGFTMRKD
 iRFP720   LTGLAIGALIGRSAADVFDSETHNRLTIALAEPGAAVGAPITVGFTMRKD
miRFP720   LTGLAIGALIGRSAADVFDSETHNRLTIALAEPGAAVGAPITVGFTMRKD

           101                                                150
 RpBphP2   AGFVGSWHRHDQLVFLELEPPQRDVAEPQAFFRRTNSAIRRLQAAETLES
 iRFP720   AGFIGSWHRHDQLIFLELEPPQRDVAEPQAFFRRTNSAIRRLQAAETLES
miRFP720   AGFIGSWHRHDQLIFLELEPPQRDVAEPQAFFRRTNSAIRRLQAAETLES

           151                                                200
 RpBphP2   ACAAAAQEVREITGFDRVMIYRFASDFSGEVIAEDRCAEVESYLGLHFPA
 iRFP720   ACAAAAQEVRKITGFDRVMIYRFASDFSGEVIAEDRCAEVESKLGLHYPA
miRFP720   ACAAAAQEVRKITGFDRVMIYRFASDFSGEVIAEDRCAEVESKLGLHYPA

           201                                                250
 RpBphP2   SDIPAQARRLYTINPVRIIPDINYRPVPVTPDLNPVTGRPIDLSFAILRS
 iRFP720   SFIPAQARRLYTINPVRIIPDINYRPVPVTPDLNPVTGRPIDLSFAILRS
miRFP720   SFIPAQARRLYTINPVRIIPDINYRPVPVTPDLNPVTGRPIDLSFAILRS

           251                                                300
 RpBphP2   VSPVHLEYMRNIGMHGTMSISILRGERLWGLIACHHRKPNYVDLDGRQAC
 iRFP720   VSPVHLEFMRNIGMHGTMSISILRGERLWGLIVCHHRTPYYVDLDGRQAC
miRFP720   VSPVHLEFMRNIGMHGTMSISILRGERLWGLIVCHHRTPYYVDLDGRQAC

           301
 RpBphP2   ELVAQVLAWQIGVMEE
 iRFP720   ELVAQVLAWQIGVMEE
miRFP720   KRVAERLATQIGVMEE
```

Amino acid sequences of miRFP720 aligned with that of the dimeric iRFP720, which was engineered from natural RpBphP2 bacterial phytochrome. Five amino acid substitutions in the iRFP720 dimerizing interface, which resulted in monomeric miRFP720, are highlighted in green.

Supplementary Figure 2. Spectral, photochemical and biochemical properties of miRFP720.

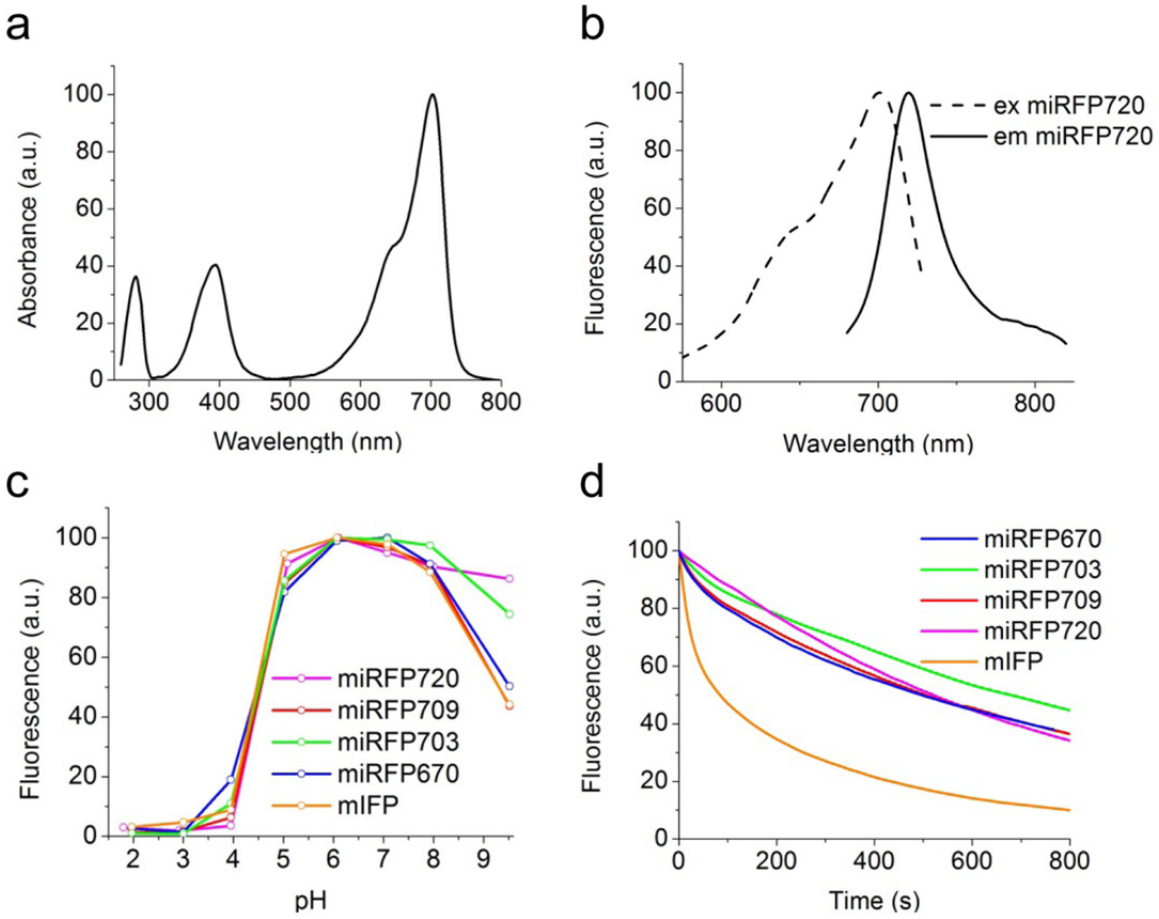

(**a**) Absorbance spectrum of miRFP720. (**b**) Excitation (dashed) and emission (solid) spectra of miRFP720. (**c**) pH dependencies of fluorescence of monomeric NIR FPs, such as miRFP670 (blue), miRFP703 (green), miRFP709 (red), miRFP720 (magenta) and mIFP (orange). (**d**) Photobleaching of monomeric NIR FPs, such as miRFP670 (blue), miRFP703 (green), miRFP709 (red), miRFP720 (magenta) and mIFP (orange), expressed in live HeLa cells. The curves were normalized to absorbance spectra and extinction coefficients of each NIR FP, spectrum of the lamp, and transmission of the excitation filter.

Supplementary Figure 3. Monomeric state of miRFP720 confirmed by analytical ultracentrifugation.

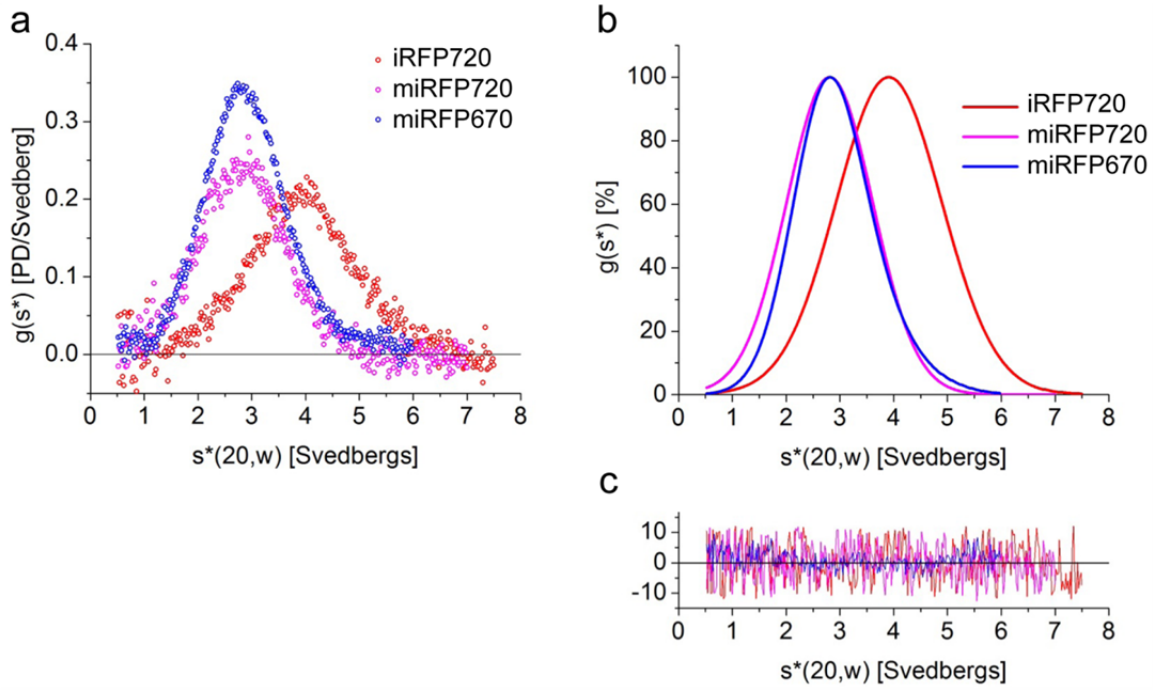

Sedimentation velocity analytical ultracentrifugation of miRFP720, compared with monomeric miRFP670 and parental dimeric iRFP720 controls run in the same conditions. The proteins were analyzed at concentrations of 15µM in PBS buffer at 20ºC, the time-derivative method was used. (**a**) Overlay of the sedimentation coefficient distributions for iRFP720 (red), miRFP720 (magenta), and miRFP670 (blue). (**b**) Overlay of the normalized best-fit sedimentation coefficient distributions. (**c**) The residuals corresponding to the resolved fits shown in (b). Monomeric fluorescent proteins showed peaks centered at a sedimentation coefficient of ~2.8-2.85 S that corresponds to the protein monomer (MW = 35 ±3kDa). The parental dimeric iRFP720 control showed the peak at ~4.0 S that corresponds to the dimer.

Supplementary Figure 4. Monomeric miRFP720 is useful as fusion tag for cellular proteins.

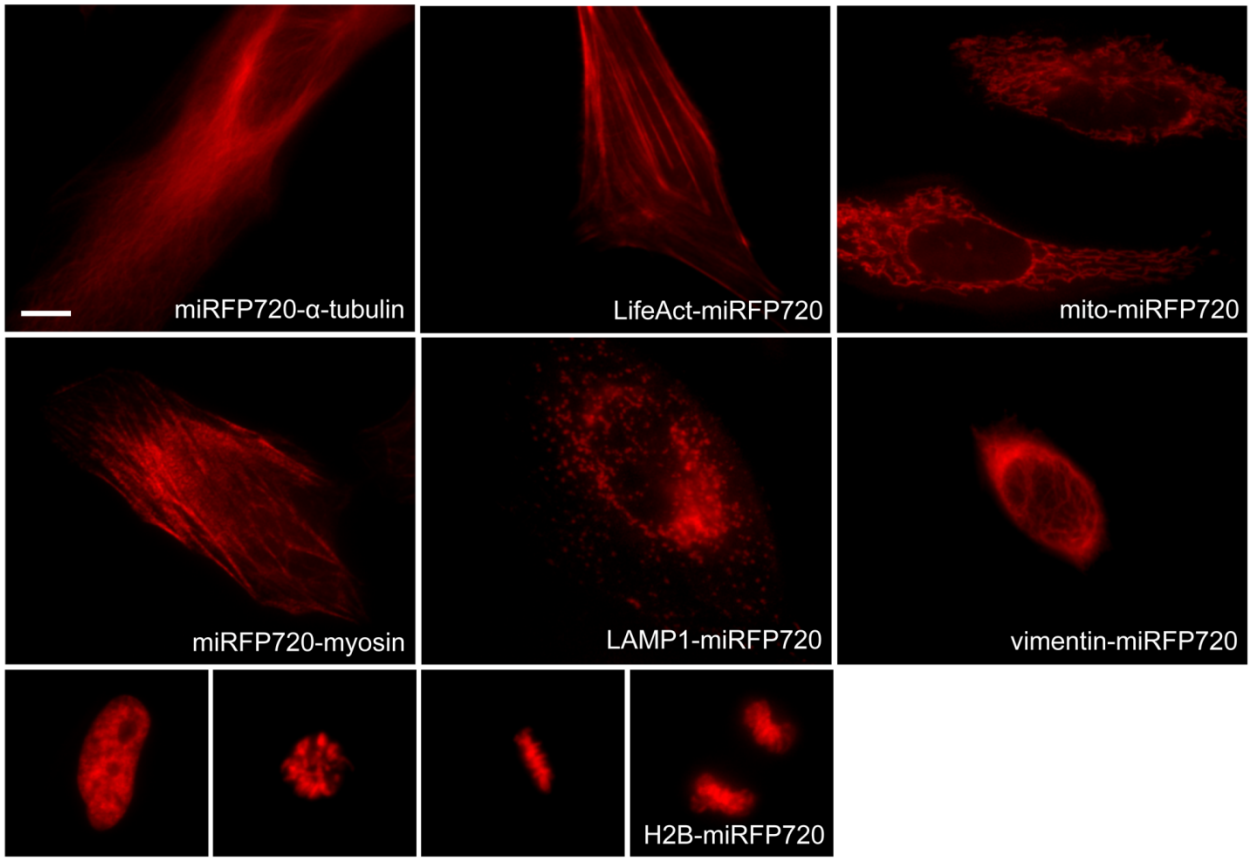

Representative NIR fluorescence images of several miRFP720 fusion constructs transiently expressed in live HeLa cells. Scale bar, 10μm. α-tubulin, LifeAct, mitochondrial targeting signal, myosin, lysosome-associated membrane protein LAMP1, vimentin, and histone 2B. Correct localization of miRFP720 fusions in filamentous structures indicated its monomeric state in live cells. The miRFP720 fusion with histone 2B show appropriate localizations during different phases of mitosis and had no effect on cell division.

Supplementary Figure 5. miRFP720 makes an effective NIR FRET pair with miRFP670.

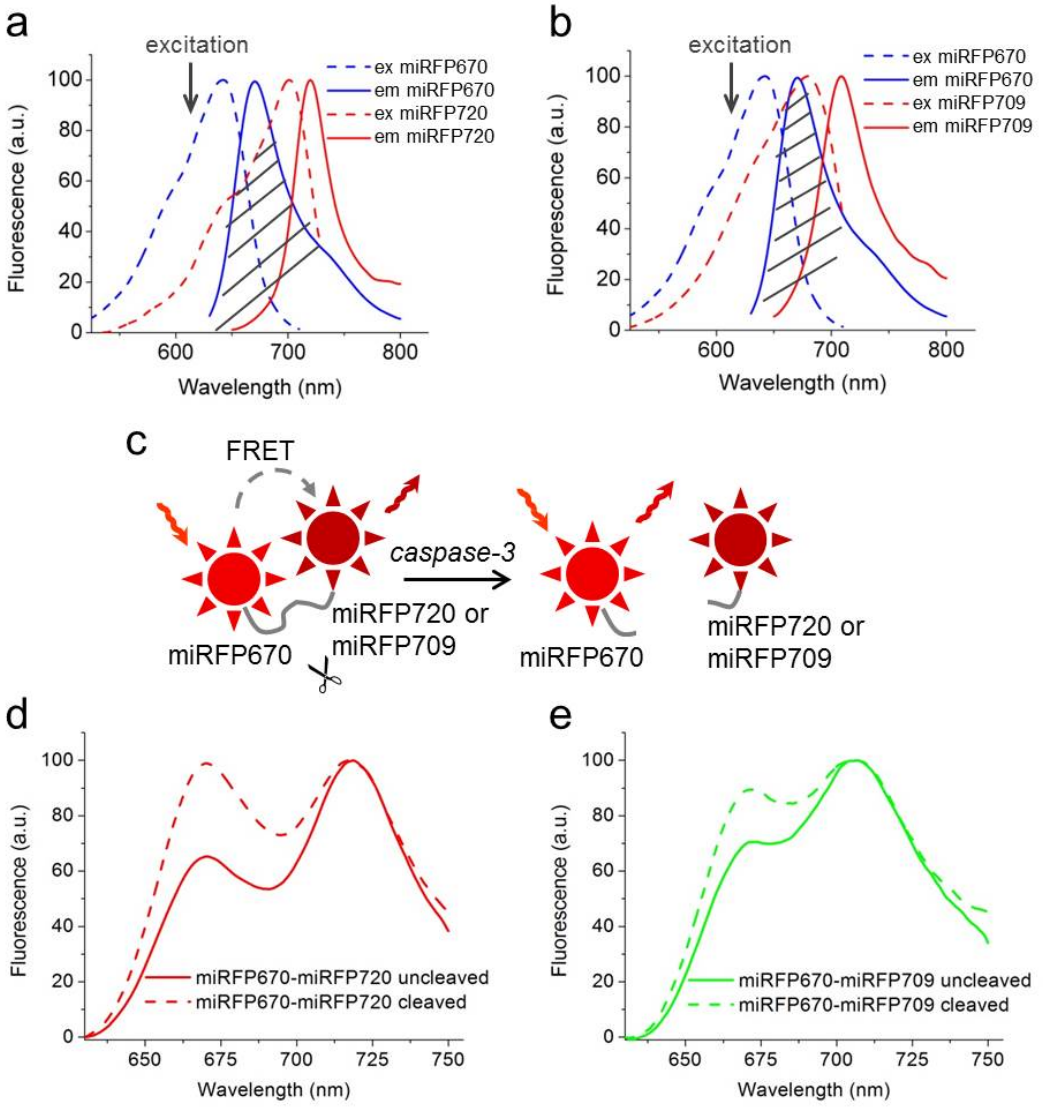

Overlay of the normalized excitation (dashed lines) and emission (solid lines) spectra for (**a**) miRFP670 donor and miRFP720 acceptor and (**b**) miRFP670 donor and miRFP709 acceptor. The arrows indicate excitation wavelengths. The shaded areas show overlaps between emission spectra of the donor and excitation spectra of the acceptor. (**c**) Schematics showing characterization of NIR FRET pairs as a caspase-3 biosensor. Emission spectra of (**d**) miRFP670-miRFP720 and (**e**) miRFP670-miRFP709 biosensors before and after cleavage by caspase-3. Fluorescence spectra were measured in a suspension of the transiently transfected HeLa cells. The spectra were acquired with 610 nm excitation and normalized to fluorescence intensity of the FRET channel (fluorescence of acceptor at 720 nm (**d**) or 709 nm (**e**)).

Supplementary Figure 6. Optimization and validation of NIR Rac1 biosensor.

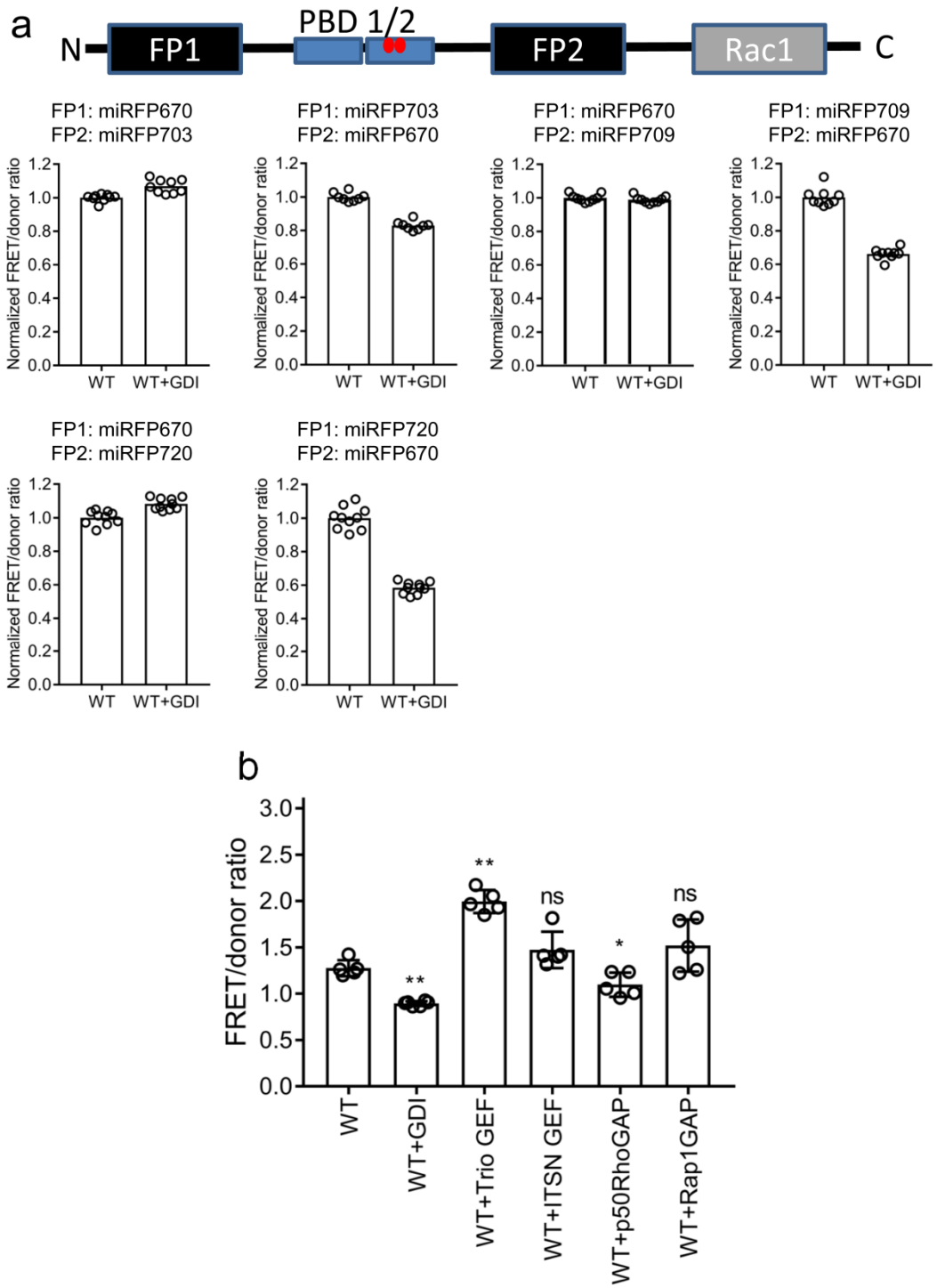

(**a**) Effect of FP orientations on FRET response, with and without the negative regulator guanine nucleotide dissociation inhibitor (GDI), measured in LinXE cells using microscopy. Data are normalized to the average wildtype response in absence of GDI. GDI was expressed at 4-fold excess to the biosensor concentration. All shown with mean. FP1-miRFP670/FP2-miRFP703: n=9 cell images from one imaging experiment; FP1-miRFP703/FP2-miRFP670: n=8 cell images

from one imaging experiment; FP1-miRFP670/FP2-miRFP709: n=9 cell images from one imaging experiment; FP1-miRFP709/FP2-miRFP670: n=9 cell images from one imaging experiment; FP1-miRFP670/FP2-miRFP720: n=10 cell images from one imaging experiment; and FP1-miRFP720/FP2-miRFP670: n=10 cell images from one imaging experiment. (**b**) Co-expression of Rac-targeting or non-Rac targeting GEFs and GAPs together with the wildtype NIR Rac1 biosensor, measured in LinXE cells using fluorometric analysis. N=5 independent experiments, shown with mean ±SEM. Student t-test (two tailed) was used. ** WT alone versus: WT+GDI, $p=2.627320\times10^{-6}$; WT+TrioGEF, $p=5.229345\times10^{-6}$. * WT alone versus: WT+p50RhoGAP, p=0.03403453. ns=not significant, WT alone versus: WT+ITSN GEF, p=0.07412487; WT+Rap1GAP, p=0.1032012. ITSN GEF: Intersectin1 guanine nucleotide exchange factor; p50RhoGAP: p50Rho GTPase-activating protein; Rap1GAP: Rap1 GTPase-activating protein.

Supplementary Figure 7. Linker optimizations for NIR-Rac1 biosensor.

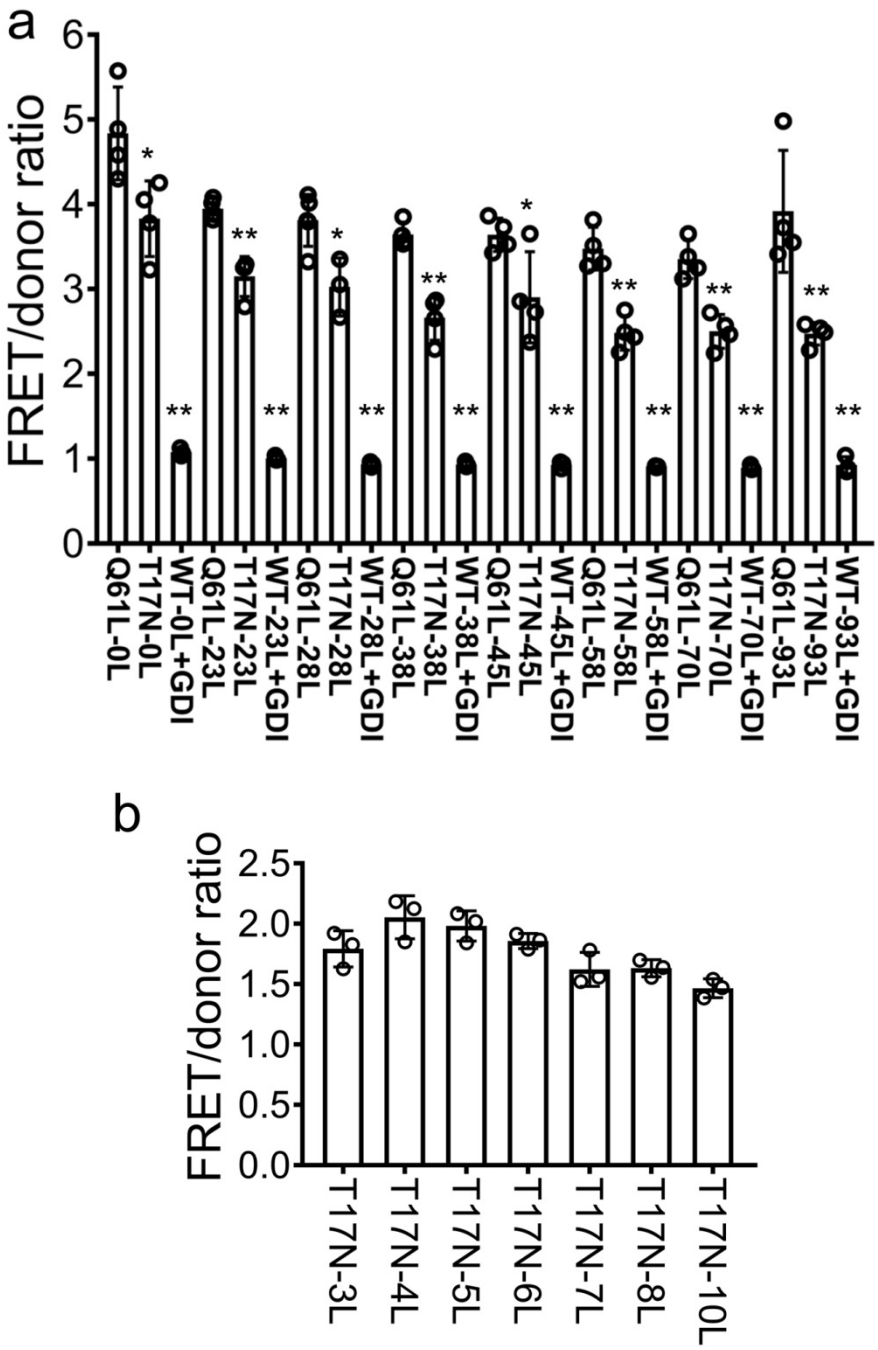

(**a**) Fluorometric analysis of adjusting the "L1" linker in the NIR Rac1 biosensor shown in **Figure 2a**, measured in LinXE cells. "L2" as shown in **Figure 2a** contains 2 amino acids encoding a restriction site. GDI plus wildtype biosensor coexpression results in low FRET/donor ratio for all linker versions. N=5 independent experiments (Q61L-28L), 4 independent experiments (Q61L-0L; T17N-0L; Q61L-23L; T17N-23L; Q61L-38L; T17N-38L; Q61L-45L; T17N-45L; Q61L-58L; T17N-58L; Q61L-70L; T17N-70L; Q61L-93L; and T17N-93L), and 3

independent experiments (T17N-28L; all conditions with GDI co-expression), shown with shown with mean ±SD. * Q61L-0L versus T17N-0L, p=0.02900744; Q61L-28L versus T17N-28L, p=0.014895308; and Q61L-45L versus T17N-45L, p=0.04259204. ** Q61L-0L versus WT-0L+GDI, $p=8.425016\times10^{-5}$; Q61L-23L versus T17N-23L, $p=9.447930\times10^{-4}$; Q61L-23L versus WT-23L+GDI, $p=1.810969\times10^{-7}$; Q61L-28L versus WT-28L+GDI, $p=4.121112\times10^{-6}$; Q61L-38L versus T17N-38L, $p=6.143420\times10^{-4}$; Q61L-38L versus WT-38L+GDI, $p=6.258947\times10^{-7}$; Q61L-45L versus WT-45L+GDI, $p=2.866537\times10^{-6}$; Q61L-58L versus T17N-58L, $p=8.633922\times10^{-4}$; Q61L-58L versus WT-58L+GDI, $p=1.207522\times10^{-5}$; Q61L-70L versus T17N-70L, $p=1.355565\times10^{-3}$; Q61L-70L versus WT-70L+GDI, $p=9.273951\times10^{-6}$; Q61L-93L versus T17N-93L, $p=7.572274\times10^{-3}$; and Q61L-93L versus WT-93L+GDI, $p=9.282299\times10^{-4}$. (**b**) Fluorometric analysis of adjusting the "L2" linker in the NIR-Rac1 biosensor shown in **Figure 2a**, measured in LinXE cells. N=3 independent experiments, shown with mean ±SEM. "L1" as shown in **Figure 2a** contains 58 amino acids.

Supplementary Figure 8. NIR Rac1 biosensor controls in cells.

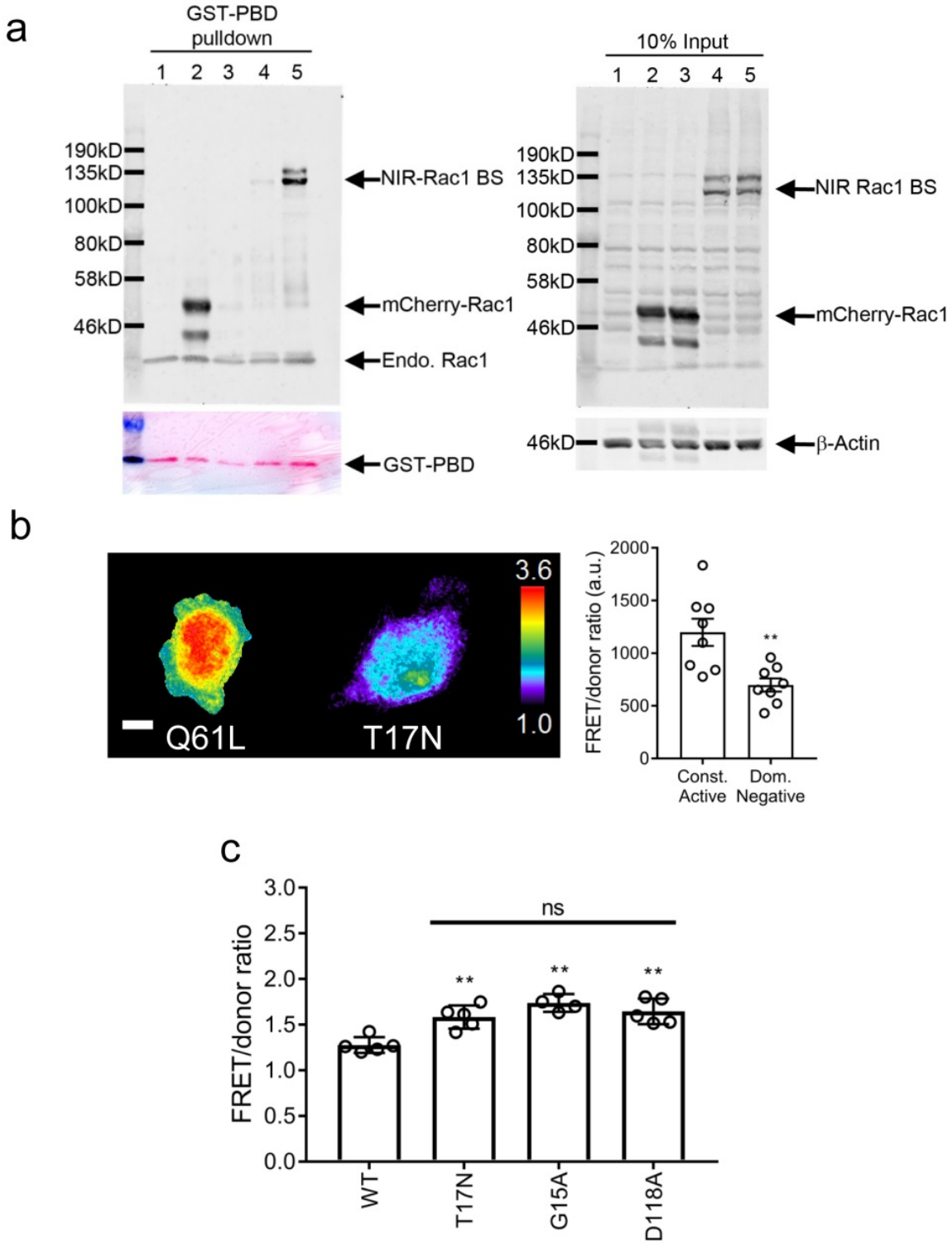

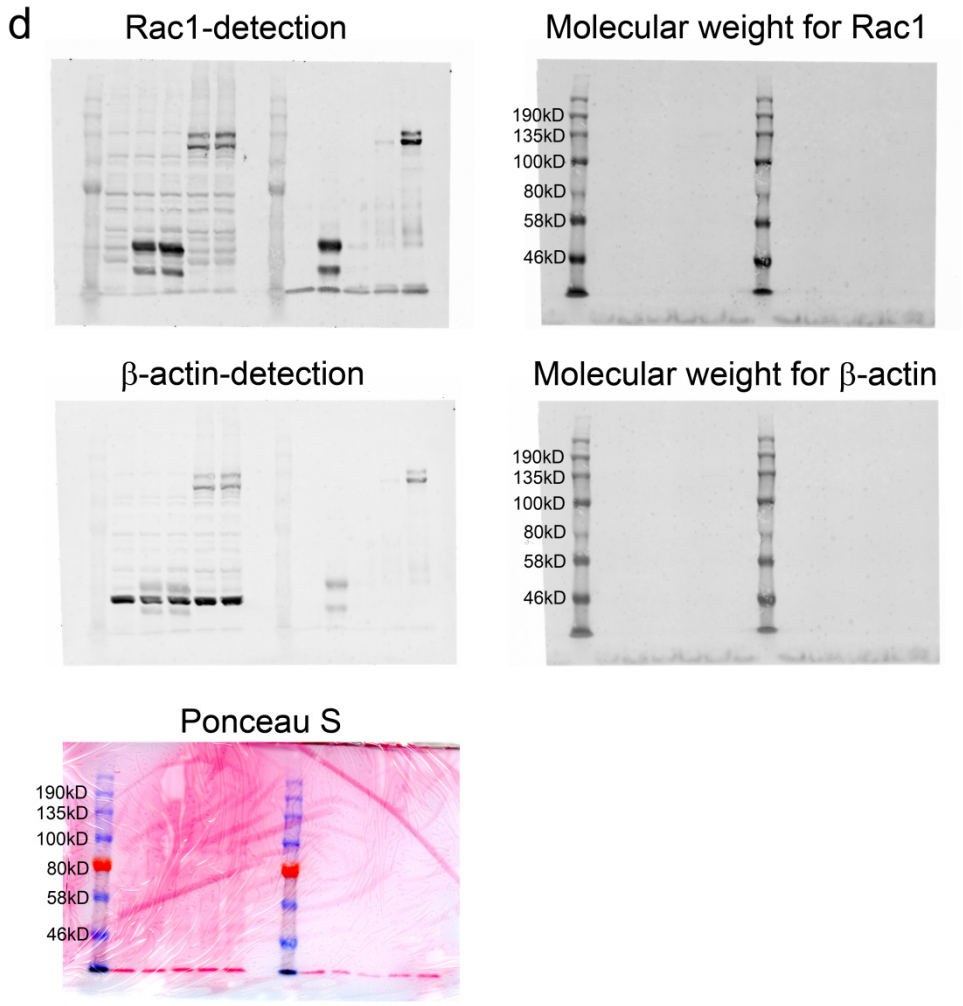

(**a**) Pulldown experiments from LinXE cell lysates using GST-PBD showing that exogenous effector domain cannot compete against binding to activated Rac1 within the biosensor. Experiments are repeated two times with similar results. Lane 1: untransfected; Lane 2: mCherry-Rac1 Q61L mutant; Lane 3: mCherry-Rac1 T17N mutant; Lane 4: NIR Rac1 biosensor with Q61L mutation; and Lane 5: NIR Rac1 biosensor with Q61L mutation and with H83/86D mutations in both PBD domains. Both main blots shown are detected using anti-Rac1 antibody. (**b**) Representative images of constitutively active or dominant negative mutant of NIR Rac1 biosensor expressed in MEF/3T3, from n=8 cells each from one experiment, with similar results. Bar = 20 µm. Student t-test (two-tailed) was used. ** $p=3.616310\times10^{-3}$, n=8 cells each from one experiment, shown with mean ±SD. (**c**) Expression of mutants of NIR Rac1 biosensor that bind GEFs non-transiently, measured in LinXE cells using fluorometric analysis. Student t-test (two-tailed) was used. ** WT (n=5 independent experiments) versus: T17N (n=5 independent experiments), $p=2.122228\times10^{-3}$; G15A (n=4 independent experiments), $p=1.366553\times10^{-4}$; and D118A (n=5 independent experiments), $p=1.003892\times10^{-3}$. ns=not significant: T17N versus G15A, p=0.08797082; T17N versus D118A, p=0.4822357; and G15A versus D118A, p=0.3043684. Data shown with mean ±SEM. (**d**) Uncropped blots from (**a**).

Supplementary Figure 9. A comparison of Rac1 biosensor based on mCerulean1-mcpVenus and the NIR Rac1 biosensor in MEF cells.

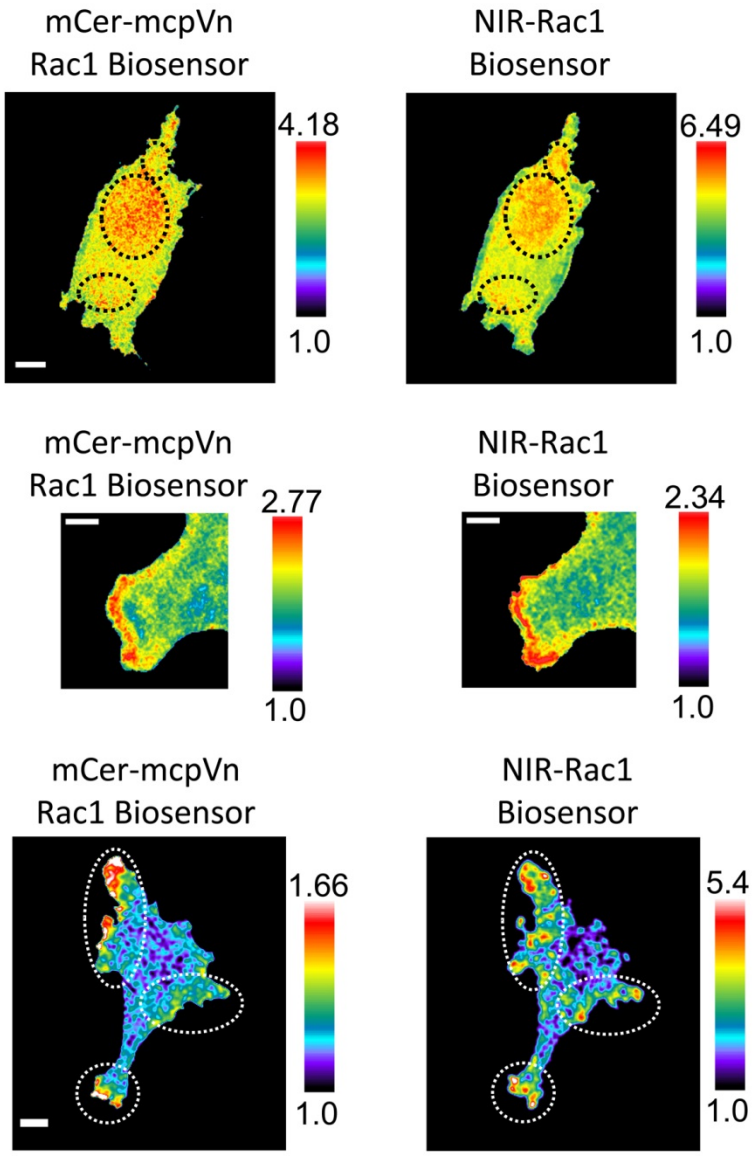

Example activities of Rac1 measured using the mCerulean1-mcpVenus Rac1 and the NIR Rac1 biosensors in the same MEF cell. N=5 independent experiments. **Upper panels:** Whole cell activities from FRET/donor ratio. Black dotted circles indicate corresponding regions of interest. White bar = 10 μm. **Middle panels:** Leading edge protrusion and an associated edge ruffle, from FRET/donor ratio. White bar = 5 μm. **Lower panels:** Whole cell activities from the subtractive correction approach ($FRET_{corrected}$=$FRET_{raw}$-α·donor-β·acceptor; where α and β are bleed-through coefficients) followed by $FRET_{corrected}$/donor ratio calculation. White dotted circles indicate corresponding regions of interest. White bar = 10 μm.

Supplementary Figure 10. Periodicity of cell edge protrusions.

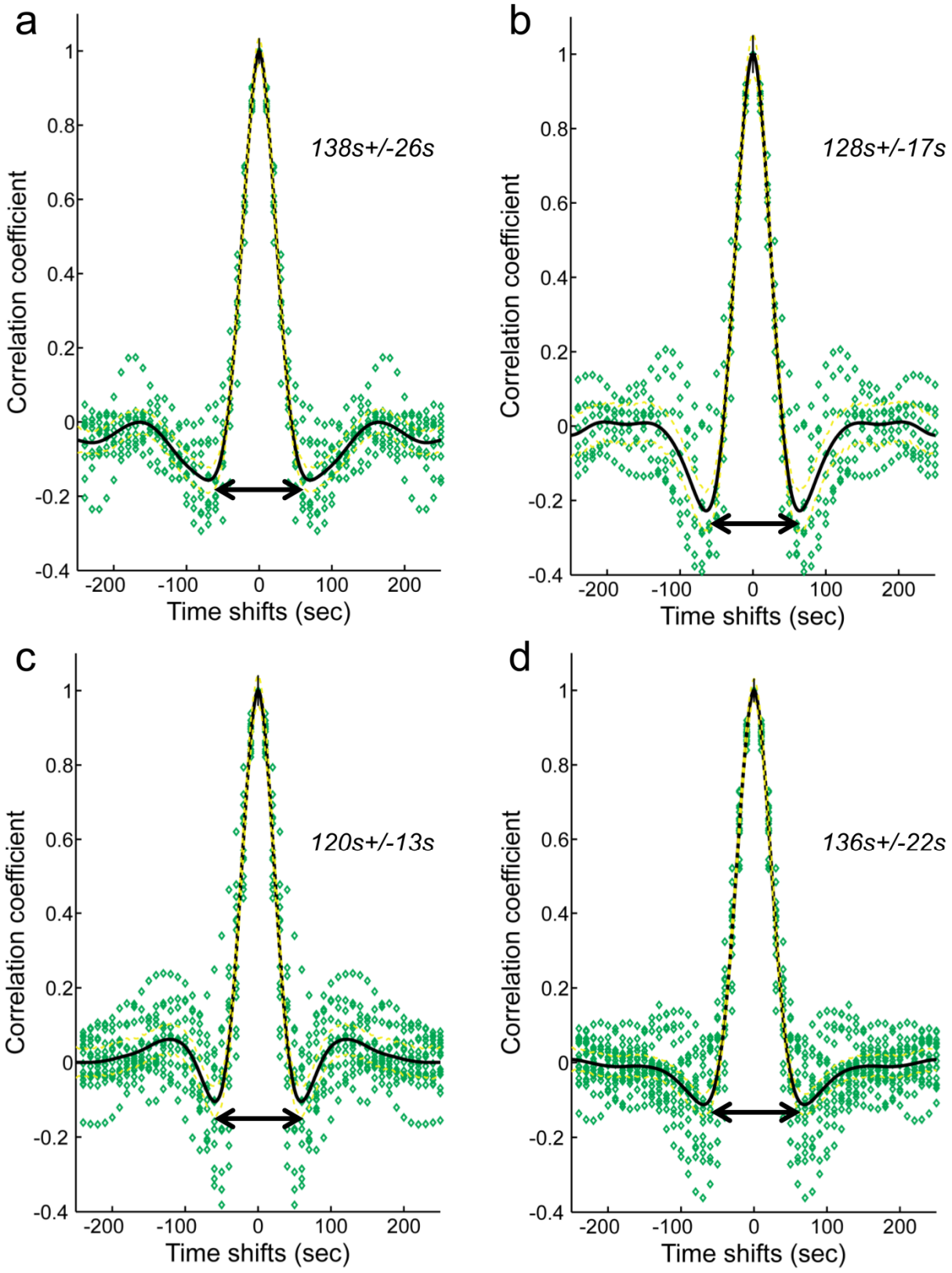

Periodicity of cell edge protrusions was measured using autocorrelation functions from the morphodynamic analysis. (**a**) MEFs expressing the RhoA biosensor [15], average of the measurements from n=560 windows from 10 cells; (**b**) Rac1 GDI/Rac1 biosensors in MEF, average of the measurements from n=827 windows from 10 cells; (**c**) RhoA/Rac1 biosensors in MEF, average of the measurements from n=1250 windows from 16 cells; and (**d**) RhoA/Rac1 biosensors in MEF under ROCK-inhibitor treatment, average of the measurements from n=990 windows from 18 cells. Black line shows the average autocorrelation function from the indicated number of cell measurements from each condition. Dashed yellow lines indicate the ±95% confidence intervals. Green open diamonds are individual data points from autocorrelation functions from each cell data. The average values provided are with ±SD. The periodicity was taken as the temporal width between the first inflections after the zero-crossing of the function, indicated with black arrow heads. Periodicities from (**b**)–(**d**) are not significantly different from (**a**) using the Student t-test (one tailed): (**a**) versus (**b**), p=0.3737767; (**a**) versus (**c**), p=0.2679213; (**a**) versus (**d**), p=0.4765897; and (**c**) versus (**d**), p=0.2656511.

Supplementary Figure 11. Rac1-RhoA activities imaged in a single MEF for the first time.

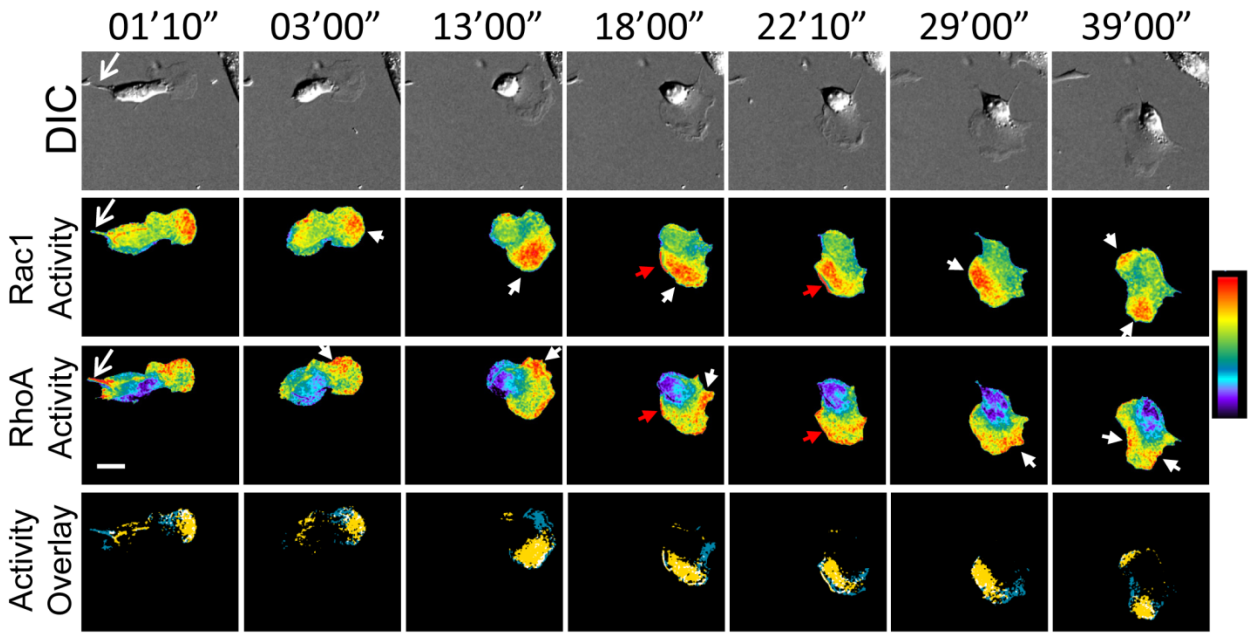

Example timelapse panels of imaging RhoA and Rac1 in a single living MEF at the same time (the first 3 time points are also shown in **Fig. 2d**), taken from data set of 16 cells from 6 independent experiments. **Top panels:** Differential interference contrast. **Middle two panels:** Rac1 and RhoA activities. **Bottom panels:** Localizations of high Rac1 (top 2.5% of activity, in yellow) and high RhoA (top 2.5% of activity, in blue) activities are overlaid, where regions of colocalization are shown in white. Regions and features of interest are indicated using matching colored arrowheads. White bar = 20 μm. Pseudocolor bar corresponds to ratio limits of 1.0 to 1.55 for Rac1 and 1.0 to 1.32 for RhoA activities (black to red).

Supplementary Figure 12. Optical characterization of NIR proteins and Rac1 biosensor.

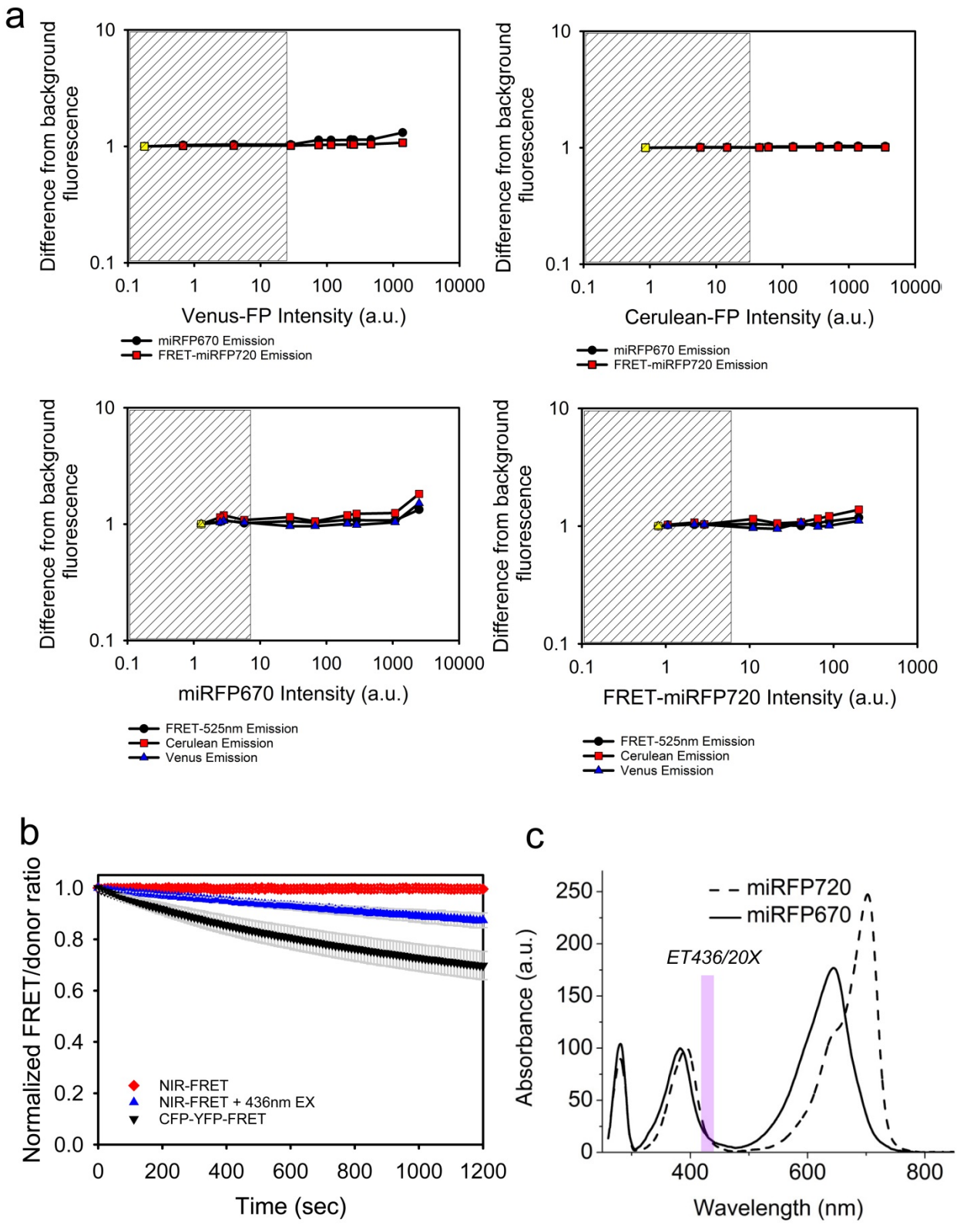

(**a**) Optical bleedthrough between different channels of fluorescence microscope used for imaging. **Top-Left:** Purified Cerulean FP fluorescence. **Top-Right:** Purified Venus FP fluorescence. **Bottom-Left:** Purified miRFP670 fluorescence. **Bottom-Right:** Purified miRFP720 fluorescence. In all panels, the first data point (yellow square) is the vehicle control (water) where no FP was present. Intensity range useful for live-cell imaging is shown as a diagonally shaded box. Data are shown with mean normalized intensity measurements from multiple fields of views and from a single experiment. Filter sets used for imaging can be found in the **Online Methods**. (**b**) Photobleach-associated changes in FRET/donor ratio as a function of time, measured in MEF cells. Whole-cell average FRET/donor ratio values are shown, from NIR-Rac1 biosensor alone excited at 628nm (Black circles), NIR-Rac1 biosensor alone with 436nm excitation in addition to 628nm excitation (Blue triangles) or CFP-YFP FRET RhoA biosensor excited at 436nm (Magenta inverted triangles), all normalized to t=0 ratio value of 1.0. The imaging medium did not contain exogenous BV. N=3 independent experiments, shown with mean ±SEM. (**c**) An overlay of absorbance spectra of miRFP670 FRET donor and miRFP720 FRET acceptor. The spectra are normalized to the peaks at ~400 nm at the Soret band. Magenta shaded region at 436nm indicates the location of the bandpass filter used for the CFP excitation (ET436/20X, Chroma Technology) during multiplex imaging.

Supplementary Figure 13. An example morphodynamic analysis from an oscillatory behavior in protrusion velocity, RhoA, and Rac1 activities in a single MEF, with or without ROCK inhibitor.

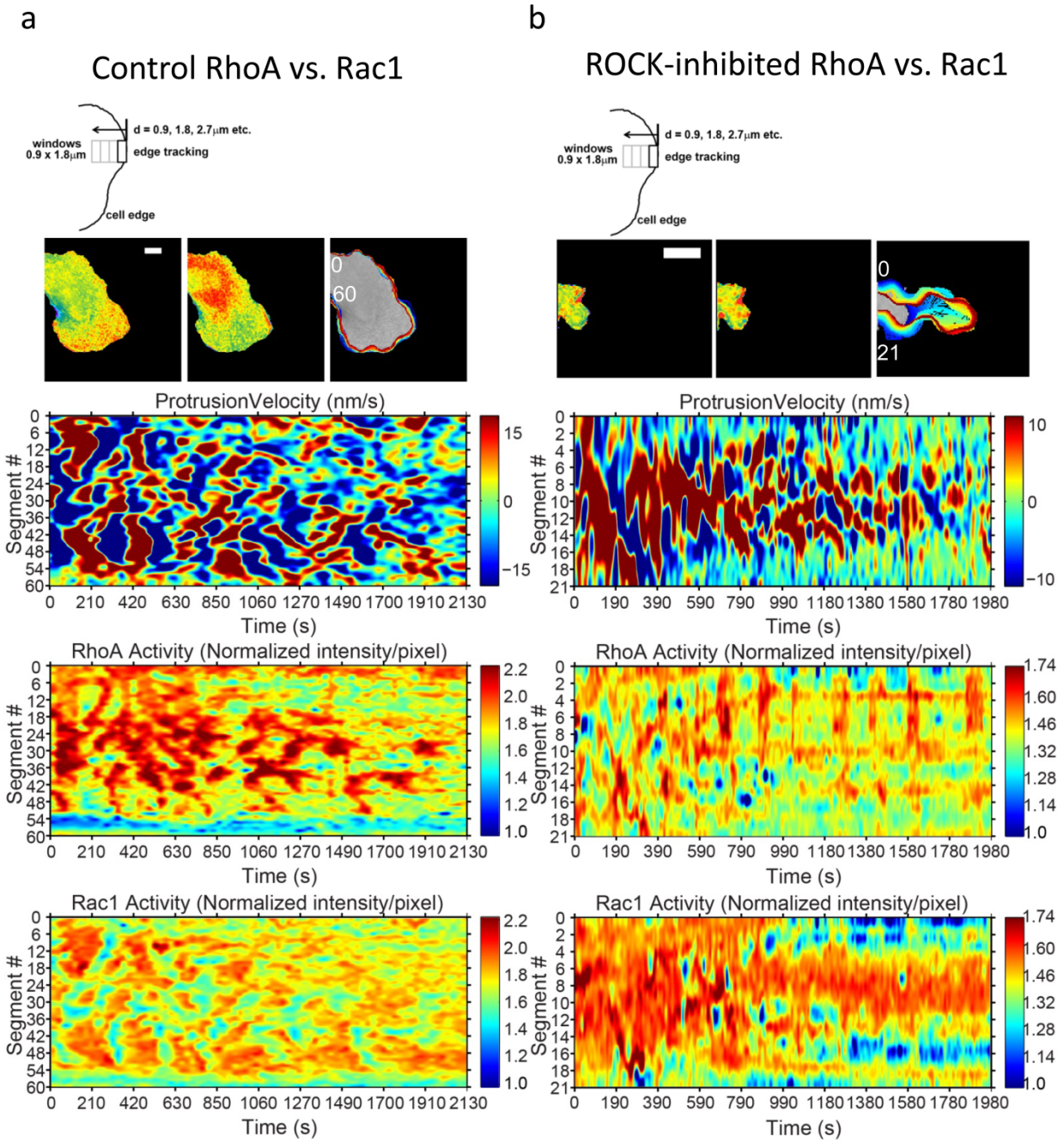

(**a**) Control morphodynamic analysis at the leading edge of MEF showing velocity, RhoA, and Rac1 activities as a function of time. (**b**) Morphodynamic analysis at the leading edge of MEF under the ROCK inhibitor treatment, showing loss of antagonistic coordination between RhoA and Rac1. The number inserts in the edge evolution panels in (**a**) and (**b**) indicate the orientation of the measurement window segments that correspond to the Y-axes of the morphodynamic maps as shown. Example images and results in (**a**) and (**b**) are taken from N=990 individual sampling window segments were measured from 18 cells, from 3 independent experiments.

Supplementary Figure 14. A model of Rac1-activation and Rac1-GDI binding during cell protrusions.

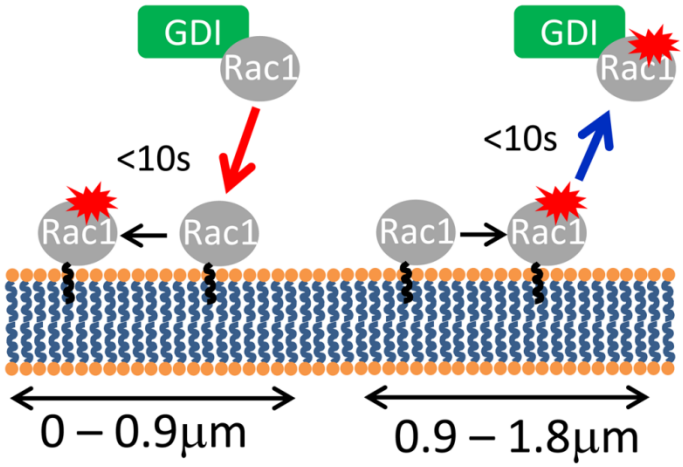

A model diagram of Rac1 activation and Rac1-GDI binding at the edge and the next adjacent region away from the edge.

Supplementary Figure 15. A timelapse panel of LOV-TRAP activation and Rac1 activity measurement in the same cell, a comparison of LOV-TRAP with TrioGEF versus Vav2 GEF catalytic domain, and effect of photoactivating LOV-TRAP on edge velocity.

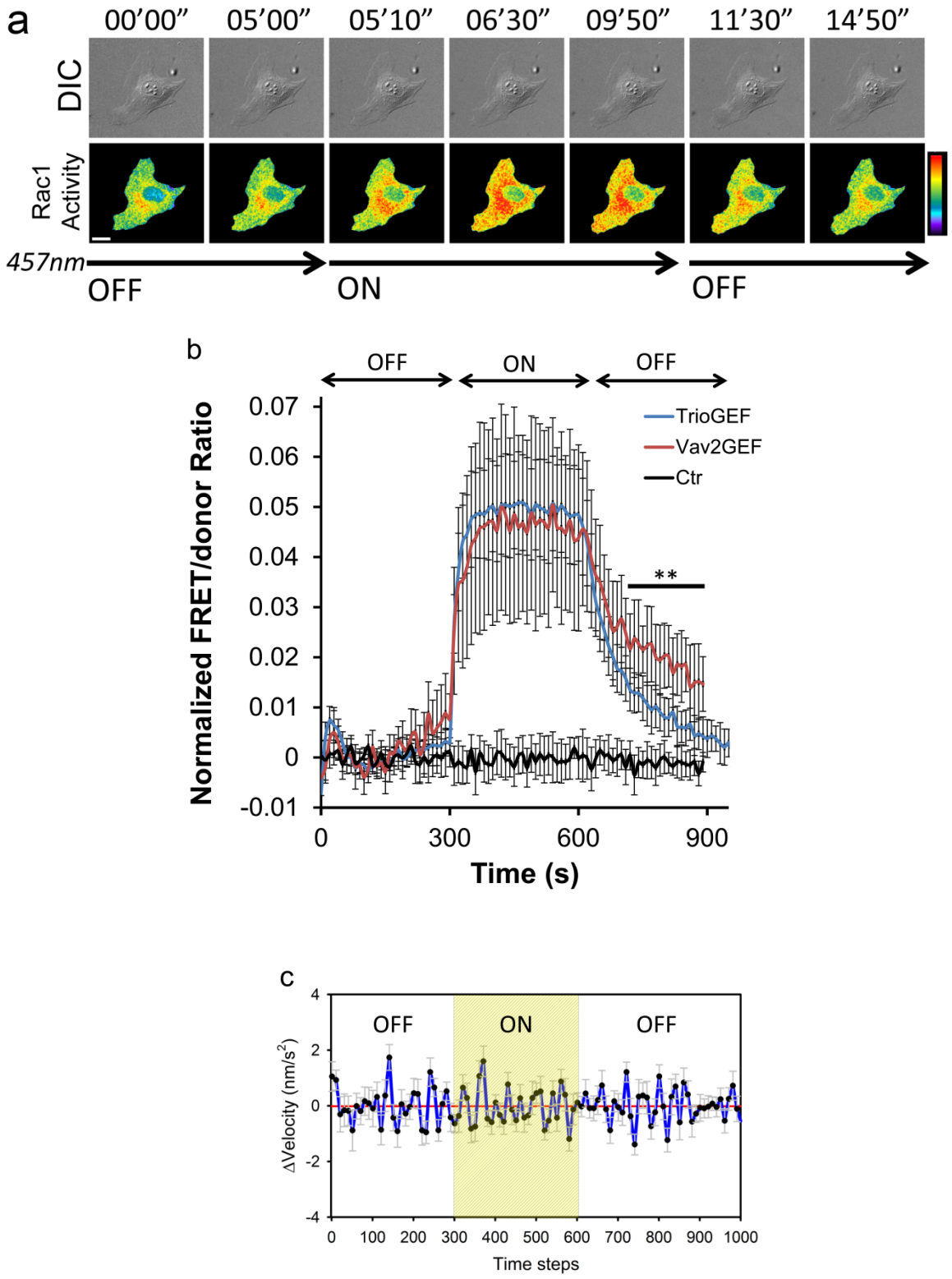

(**a**) A Representative panel of a MEF undergoing photoactivation of LOV-TRAP and a concurrent measurement of Rac1 activity using the NIR-Rac1 biosensor. NIR-Rac1 biosensor images were acquired every 10 s. 457nm illumination consisted of cycles of 4s-on, 6s-off at indicated times (select time points are also shown in **Fig. 5B**). White bar=20 μm. Pseudocolor limits are 1.0 to 1.74 (black to red). Example taken from N=17 independent photoactivation experiments. (**b**) The original Vav2 GEF LOV-TRAP results in slower decay of Rac1 activity during the dark relaxation compared to the TrioGEF LOV-TRAP, measured in MEF cells, all shown with mean ±SEM (Vav2 GEF: 10 independent photoactivation experiments; TrioGEF: 17 independent photoactivation experiments; control: 10 independent mock-photoactivation experiments). Student t-test was used (two tailed) comparing Rac1 activity levels between TrioGEF versus Vav2 GEF: ** at 730s, $p=2.947164\times10^{-3}$; 740s, $p=8.402130\times10^{-3}$; 750s, $p=2.269420\times10^{-3}$; 760s, $p=2.575764\times10^{-3}$; 770s, $p=1.140031\times10^{-3}$; 780s, $p=3.856585\times10^{-3}$; 790s, $p=1.898763\times10^{-3}$; 800s, $p=3.415040\times10^{-4}$; 810s, $p=2.159023\times10^{-4}$; 820s, $p=1.343570\times10^{-2}$; 830s, $p=2.928501\times10^{-4}$; 840s, $p=2.386960\times10^{-4}$; 850s, $p=5.087652\times10^{-5}$; 860s, $p=2.700972\times10^{-2}$; 870s, $p=3.808177\times10^{-3}$; 880s, $p=1.730448\times10^{-3}$; 890s, $p=8.129790\times10^{-4}$. (**c**) The release of activated GEF domain of TrioGEF using LOV-TRAP results in no apparent change to the edge acceleration as a function of time, shown with mean ±SEM. The data were calculated from averaged velocity differentials, taken from n=1432 individual windows from 17 independent photoactivation experiments, measured in MEF cells. Using the Student t-test (two tailed) and comparing 0s-300s versus 300s-600s, p=0.6436633; 0s-300s versus 600s-1000s, p=0.9328191; and 0s-300s versus 600s-1000s, p=0.7230980, indicated there were no significant differences.

Supplementary Figure 16. Timelapse panels of AKAR and JNKAR biosensors based on NIR FRET, using NIR miRFP670-miRFP720 FRET pair.

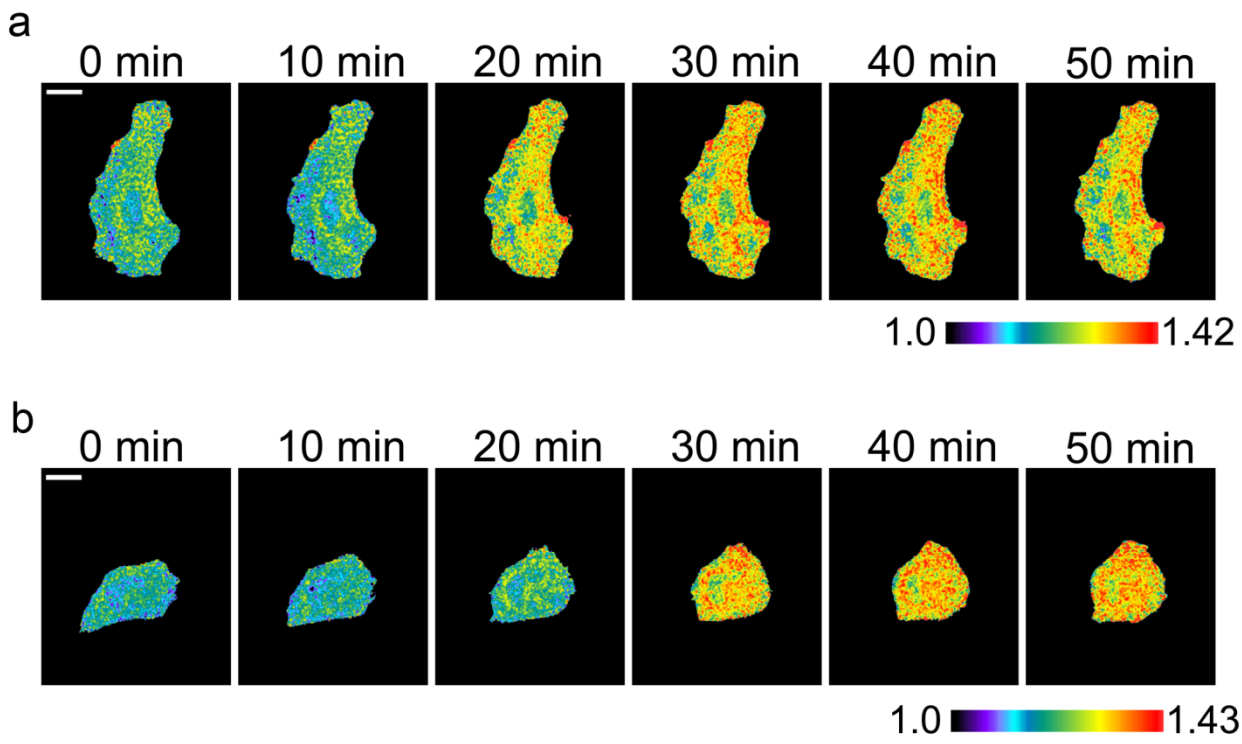

(**a**) Representative timelapse images of a HeLa cell expressing the NIR-AKAR PKA sensor and undergoing stimulation. 1 mM dbcAMP was added at the 10 min time point and the FRET/donor ratio was monitored for up to 70 min (select time points are also shown in **Fig. 6b**). White bar = 20 µm. Example image set taken from n=3 stimulation experiments. (**b**) Representative time-lapse images of a HeLa cell expressing the NIR-JNKAR JNK sensor and undergoing stimulation. 1 µg/mL anisomycin was added at the 10 min time point and the FRET/donor ratio was monitored for up to 70 min (select time points are also shown in **Fig. 6d**). White bar = 20 µm. Example image set taken from n=3 stimulation experiments.

Supplementary Video 1. A representative live cell movie of a control MEF cell with CFP-YFP FRET RhoA and NIR Rac1 biosensors imaged concurrently. Differential interference contrast, RhoA activity, Rac1 activity, and binary overlay of high RhoA/Rac1 activities are shown (yellow: top 2.5% of Rac1 activity; blue: top 2.5% of RhoA activity; white: colocalization). White bar = 20 μm. Frame rate: 7 frames per second, timelapse imaging rate: 10 s intervals. Example cell taken from data set of 16 cells from 6 independent experiments.

Supplementary Video 2. A representative segment of a leading edge protrusion used in morphodynamic analysis from control MEF cell with CFP-YFP FRET RhoA and NIR Rac1 biosensors imaged concurrently. RhoA activity, Rac1 activity, and binary overlay of high RhoA/Rac1 activities are shown (yellow: top 6% of Rac1 activity; blue: top 6% of RhoA activity; white: colocalization). White bar = 10 μm. Frame rate: 7 frames per second, timelapse imaging rate: 10 s intervals. Example cell taken from data set of 16 cells, from 6 independent experiments.

Supplementary Video 3. A representative segment of a leading edge protrusion used in morphodynamic analysis from control MEF cell with CFP-YFP FRET RhoA and NIR Rac1 biosensors imaged concurrently. RhoA activity, Rac1 activity, and binary overlay of high RhoA/Rac1 activities are shown (yellow: top 5.5% of Rac1 activity; blue: top 5.5% of RhoA activity; white: colocalization). White bar = 10 μm. Frame rate: 7 frames per second, timelapse imaging rate: 10 s intervals. Example cell taken from data set of 16 cells, from 6 independent experiments.

Supplementary Video 4. A representative segment of a leading edge protrusion used in morphodynamic analysis from MEF cell treated with ROCK-inhibitor, with CFP-YFP FRET RhoA and NIR Rac1 biosensors imaged concurrently. RhoA activity, Rac1 activity, and binary overlay of high RhoA/Rac1 activities are shown (yellow: top 8% of Rac1 activity; blue: top 8% of RhoA activity; white: colocalization). White bar = 10 μm. Frame rate: 7 frames per second, timelapse imaging rate: 10 s intervals. Example cell taken from data set of 18 cells, from 3 independent experiments.

Supplementary Video 5. A representative segment of a leading edge protrusion used in morphodynamic analysis from MEF cell treated with ROCK-inhibitor, with CFP-YFP FRET RhoA and NIR Rac1 biosensors imaged concurrently. RhoA activity, Rac1 activity, and binary overlay of high RhoA/Rac1 activities are shown (yellow: top 3% of Rac1 activity; blue: top 3% of RhoA activity; white: colocalization). White bar = 10 μm. Frame rate: 7 frames per second, timelapse imaging rate: 10 s intervals. Example cell taken from data set of 18 cells, from 3 independent experiments.

Supplementary Video 6. A representative segment of a leading edge protrusion used in morphodynamic analysis from MEF cell with CFP-YFP FRET Rac1-GDI binding biosensor and NIR Rac1 biosensors imaged concurrently. Rac1-GDI binding, Rac1 activity, and binary overlay of high Rac1-GDI binding/Rac1 activity are shown (yellow: top 5% of Rac1 activity; blue: top 5% of Rac1-GDI binding; white: colocalization). White bar = 10 μm. Frame rate: 7 frames per second, timelapse imaging rate: 10 s intervals. Example cell taken from data set of 10 cells from 3 independent experiments.

Supplementary Video 7. A representative live cell movie of LOV-TRAP optogenetics of Rac1 activity and concurrent measurement of Rac1 activity using the NIR Rac1 biosensor in a MEF cell. 457 nm light was used to illuminate the whole field of view during indicated time points. White bar = 20 μm. Frame rate: 7 frames per second, timelapse imaging rate: 10 s intervals. Example cell taken from data set of 17 independent photoactivation experiments.

Supplementary Video 8. A representative live cell movie of a HeLa cell with AKAR biosensor. White bar = 20 μm. Frame rate: 7 frames per second, timelapse imaging rate: 2 min intervals. * indicates addition of 1 mM dbcAMP. Example cell taken from data set of 3 independent stimulation experiments.

Supplementary Video 9. A representative live cell movie of a HeLa cell with JNKAR biosensor. White bar = 20 μm. Frame rate: 7 frames per second, timelapse imaging rate: 2 min intervals. * indicates addition of 1 μg/mL anisomycin. Example cell taken from data set of 3 independent stimulation experiments.

Supplementary Material Reference

50. Yu, D. et al. A naturally monomeric infrared fluorescent protein for protein labeling in vivo. *Nat Methods* **12**, 763-5 (2015).